Electronic Supplementary Material (ESI) for Dalton Transactions.

Complexes of tin(II) phthalocyanine in neutral and radical anion states with transition metal carbonyl clusters: methods of synthesis, structures and properties.

Nikita R. Romanenko,[a] Alexey V. Kuzmin,[b] Salavat S. Khasanov,[b] Maxim A. Faraonov,[a] Evgeniya I. Yudanova,[a] Yoshiaki Nakano,[c,d] Akihiro Otsuka,[c, d] Hideki Yamochi,[c,d] Hiroshi Kitagawa,[c] and Dmitri V. Konarev[a*]

[a]Institute of Problems of Chemical Physics RAS, Chernogolovka, Moscow region, 142432 Russia;

[b]Institute of Solid State Physics RAS, Chernogolovka, Moscow region, 142432 Russia;

[c]Division of Chemistry, Graduate School of Science, Kyoto University, Sakyo-ku, Kyoto 606-8502, Japan;

[d]Research Center for Low Temperature and Materials Sciences, Kyoto University, Sakyo-ku, Kyoto 606-8501, Japan.

EXPERIMENTAL

Materials. Tin(II) and tin(IV) dichloride phthalocyanines ($Sn^{II}Pc$ and $Sn^{IV}Cl_2Pc$, respectively, >98%), tetracobalt dodecacarbonyl ($Co_4(CO)_{12}$, >98%), dicobalt octacarbonyl ($Co_2(CO)_8$, stabilized with 1-5% of *n*-hexane), iridium carbonyl ($Ir_4(CO)_{12}$, >98%), ruthenium carbonyl ($Ru_3(CO)_{12}$, >99%), osmium carbonyl ($Os_3(CO)_{12}$, >99%), decamethylchromocene (Cp^*_2Cr, >95%), and potassium graphite (KC_8) were purchased from Strem. Cryptand[2.2.2] (herafter abbreviated as Cryptand) was purchased from Acros. Sodium fluorenone ketyl was obtained according to Ref. [1]. Cesium anthracenide was obtained according to Ref. [2]. *o*-Dichlorobenzene ($C_6H_4Cl_2$, 99%) was distilled over CaH_2 under reduced pressure in argon atmosphere, and *n*-hexane was distilled over Na/benzophenone in argon atmosphere. Solvents were degassed and stored in an MBraun 150B-G glove box. Complexes **1** - **6** were synthesized and stored in the glove box with controlled atmosphere containing less than 1 ppm of water and oxygen. KBr pellets used for the IR and UV-visible-NIR analyses of **1-5** were prepared in the glove box. Magnetic measurements were performed on carefully purified and tested crystals of **1**, **2**, **4** and **5** sealed in a 2 mm quarz tube under ambient pressure of argon.

General. UV-visible-NIR spectra were measured in KBr pellets on a PerkinElmer Lambda 1050 spectrometer in the 250-2500 nm range. FT-IR spectra were obtained in KBr pellets with a PerkinElmer Spectrum 400 spectrometer (400-7800 cm^{-1}). EPR spectra were recorded for a polycrystalline sample of **1**, **2**, **4** and **5** from room temperature (295 K) down to liquid helium temperature with a JEOL JES-TE 200 X-band ESR spectrometer equipped with a JEOL ES-CT470 cryostat. A Quantum Design MPMS-XL SQUID magnetometer was used to measure static magnetic susceptibilities of **1**, **2**, **4** and **5** at 100 mT magnetic field in cooling and heating conditions in the 300 − 1.9 K range. A sample holder contribution and core temperature independent diamagnetic susceptibility (χ_d) were subtracted from the experimental data. The χ_d values were estimated by the extrapolation of the data in the high-temperature range by fitting the data with the following expression: $\chi_M = C/(T - \Theta) + \chi_d$, where C is Curie constant

and Θ is Weiss temperature. Effective magnetic moment (μ_{eff}) was calculated with the following formula: $\mu_{eff} = (8 \cdot \chi_M \cdot T)^{1/2}$

Synthesis. Crystals of **1**-**6** were obtained by diffusion technique. The obtained solutions were cooled down to room temperature and filtered into the 1.8-cm-diameter, 50 mL glass tube with a ground glass plug, and then 24 mL of *n*-hexane was layered over the solution. Slow mixing of the solutions over 1-1.5 months resulted in precipitation of crystals. The solvent was then decanted from the crystals, and they were washed with *n*-hexane.

Crystals of $\{Co_4(CO)_{11} \cdot Sn^{II}(Pc^{2-})\}$ (**1**) were obtained via the interaction of $Sn^{II}Pc$ (26.6 mg, 0.042 mmol) with 2.2 equivalents of $Co_2(CO)_8$ (31.1 mg, 0.046 mmol) in *o*-dichlorobenzene upon stirring the solution during one day at 60^{o}C. Phthalocyanine was completely dissolved to form deep green solution. After slow mixing with *n*-hexane black crystals were obtained in 65% yield. As it was discussed in the main text, this sample contained impurity of metallic cobalt which manifested broad EPR signals. Alternative method of the synthesis of **1** was an interaction of $Sn^{II}Pc$ (26.6 mg, 0.042 mmol) and one equivalent of $Co_4(CO)_{12}$ (23.9 mg, 0.042 mmol) during one day at room temperature. Phthalocyanine completely dissolved to form deep green solution. After slow mixing with *n*-hexane black prisms were obtained in 71% yield. Analysis of the unit cell parameters of obtained crystals in both synthesis showed that they are isostructural and have the same IR and UV-visible-NIR spectra. However, measurements of EPR spectra at room and liquid helium temperatures indicated the absence of any EPR signals and, therefore, second syntheses allowed us to obtain EPR silent crystals of **1** without impurities. Elemental analysis confirmed the composition of **1** determined from X-ray diffraction: $C_{43}H_{16}Co_4N_8O_{11}Sn$, M_r = 1175.05 g mol^{-1}: Calcd. C = 43.95, H = 1.36, N = 9.53%; Found: C = 43.12, H = 1.28, N = 9.18%.

For preparation of $\{Cryptand(Na^+)\}\{Ru_3(CO)_{11} \cdot Sn^{II}(Pc^{\bullet 3-})\}^-$ (**2**), salt $\{Cryptand(Na^+)\}\{Sn^{II}(Pc^{\bullet 3-})\}^-$ was generated in solution. $Sn^{II}Pc$ (26.6 mg, 0.042 mmol) was reduced by slight excess of sodium fluorenone ketyl ($C_{13}H_8ONa$) (11.4 mg, 0.056 mmol) in the presence of one equivalent of Cryptand (16 mg, 0.042 mmol) in 17 ml of *o*-dichlorobenzene during one day at 60^{o}C. Phthalocyanine completely dissolved to form deep blue solution which was cooled down to room temperature and filtered into the

flask containing 26.7 mg of $Ru_3(CO)_{12}$ (0.042 mmol). Solution was stirred for one more day at 60°C, and colour of the solution remained unchanged. Solution was cooled down to room temperature and filtered into a tube for diffusion. Large black crystals precipitated after slow mixing with *n*-hexane during 1 month. Solvent was decanted and crystals were washed by *n*-hexane to yield black blocks with copper lustre characteristic of reduced phthalocyanines. The yield of crystals was 56%.

Similar reactions were carried out for $Co_4(CO)_{12}$ and $Ir_4(CO)_{12}$ clusters. Addition of $\{Cryptand(Na^+)\}\{Sn^{II}(Pc^{\bullet 3-})\}^-$ salt to $Co_4(CO)_{12}$ provided color change from deep blue to green. No crystals were obtained in this case after slow mixing with *n*-hexane. On the contrary, upon mixing of $\{Cryptand(Na^+)\}\{Sn^{II}(Pc^{\bullet 3-})\}^-$ with $Ir_4(CO)_{12}$ deep blue color remained unchanged, and black crystals were obtained after slow mixing with *n*-hexane. However, structure of these crystals was not solved at 100 K completely by the X-ray diffraction analysis due to strong disorder observed even for a slowly cooled crystal. Therefore, we cannot discuss this product.

Salt $\{Cryptand(M^+)\}\{Sn^{II}(Pc^{\bullet 3-})\}^-$ was initially generated in solution for preparation of $\{Cryptand(M^+)\}_2\{Ru_3(CO)_{10}\cdot[Sn^{II}(Pc^{\bullet 3-})]_2\}^{2-}\cdot 4C_6H_4Cl_2$ (M^+ is K or Cs). $Sn^{II}Pc$ (26.6 mg, 0.042 mmol) was reduced by mixture of reductants (potassium graphite (KC_8) (10 mg, 0.148 mmol) and cesium anthracenide (10 mg, 0.032 mmol)) in the presence of one equivalent of Cryptand (16 mg, 0.042 mmol) in 17 ml of *o*-dichlorobenzene during one day at 60°C. Phthalocyanine completely dissolved to form deep blue solution. It was cooled down to room temperature and filtered into the flask containing half equivalent of 13.4 mg of $Ru_3(CO)_{12}$ (0.021 mmol). Solution was stirred for one more day at 60°C (color of the solution remained unchanged). Solution was cooled down to room temperature and filtered into a tube for diffusion. Crystals precipitated after slow mixing with *n*-hexane during 1.5 months. Solvent was decanted and crystals were washed by *n*-hexane to yield dark black plates with copper lustre characteristic of reduced phthalocyanines. The yield of pure crystals was rather low (only several milligrams). Similarly, we also carried out experiment with a ($\{Sn^{II}(Pc^{\bullet 3-})\}^-$: $Ru_3(CO)_{12)}$ = 3:1 ratio but no new crystal phase formed in this case.

For the synthesis of $(Cp^*_2Cr^+)\{Ru_3(CO)_{11}\cdot Sn^{II}(Pc^{\bullet 3-})\}^-\cdot C_6H_4Cl_2$ (**4**) cluster $Ru_3(CO)_{12}$ (26.7 mg, 0.042 mmol) was reduced by slight excess of Cp^*_2Cr (15 mg, 0.046 mmol) in *o*-dichlorobenzene by stirring the solution during one day at 80°C. Color of the solution changed from orange to red-brown and orange powder of $Ru_3(CO)_{12}$ dissolved. Obtained solution is filtered into the flask containing half equivalent of $Sn^{IV}Cl_2Pc$ (14.7 mg, 0.021 mmol). Solution is stirred at 60°C for one day more to yield deep blue solution. Slow mixing of the obtained solution with *n*-hexane yields black blocks with characteristic for reduced phthalocyanines copper luster. The yield of the crystals is 42%. Testing of the crystals by X-ray diffraction show that only one crystal phase is formed.

When we studied reduction of $Os_3(CO)_{12}$ (37.8 mg, 0.042 mmol) by decamethylchromocene (15 mg, 0.046 mmol) no crystals suitable for X-ray diffraction were isolated.[4] However, the interaction of the reduced species with half equivalent of $Sn^{IV}Cl_2Pc$ (14.7 mg, 0.021 mmol) by stirring of the solution at 60°C yielded deep blue solution from which slow mixing with *n*-hexane yields black blocks suitable for X-ray structure analysis. Composition of the crystals according to this analysis was $(Cp^*_2Cr^+)\{Os_3(CO)_{10}Cl\cdot Sn^{II}(Pc^{\bullet 3-})\}^-\cdot C_6H_4Cl_2$ (**5**). Crystals with characteristic for reduced phthalocyanines copper luster were obtained in 47% yield. Testing of the crystals by X-ray diffraction show that only one crystal phase is formed and these crystals were taken to carry out the study of their optical and magnetic properties.

For synthesis of $(Cp^*_2Cr^+)\{Ir_4(CO)_{11}\cdot Sn^{II}(Pc^{\bullet 3-})\}_2^-$ (**6**) initially cluster $Ir_4(CO)_{12}$ (46.1 mg, 0.042 mmol) was reduced by slight excess of Cp^*_2Cr (15 mg, 0.046 mmol) in *o*-dichlorobenzene by stirring the solution during one day at 80°C. Color of the solution changed to red, and yellow powder of $Ir_4(CO)_{12}$ dissolved. In this case obtained solution was filtered into a flask containing half equivalent of $Sn^{IV}Cl_2Pc$ (14.7 mg, 0.021 mmol). Solution was stirred for one more day at 60°C to yield deep blue-green solution at complete dissolution of phthalocyanine. Slow mixing of the obtained solution with *n*-hexane yielded small crystals in form of black blocks. Testing of the obtained crystals by X-ray diffraction showed the presence of two phases. New phase (**6**) studied by X-ray diffraction has the $(Cp^*_2Cr^+)\{Ir_4(CO)_{11}\cdot Sn^{II}(Pc^{\bullet 3-})\}^-$ composition. Second phase according to the unit cell parameters was

previously studied complex of the reduced $Ir_4(CO)_{12}$ -$(Cp^*_2Cr^+)_2\{Ir_8(CO)_{18}\}^{2-}$.[3] Crystals of two phases could not be safely separated due to their small size. Therefore, we present only crystal structure of **6**.

Elemental analysis could not be used to confirm the composition of **2-5** due to extremely high air-sensitivity of obtained crystals. Due to oxidation of $Pc^{\bullet 3-}$ in the presence of transition metals, addition of oxygen during the procedure of elemental analysis was observed, which changed the content of elements in the samples. Therefore, their composition was determined from X-ray diffraction on single crystals only.

X-ray crystal structure determination

X-ray diffraction data for **1-6** are listed in Tables S1 and S2. X-ray diffraction data for **1-6** were collected on an Oxford diffraction "Gemini-R" CCD diffractometer with graphite monochromated MoK_α radiation using an Oxford Instrument Cryojet system. Raw data reduction to F^2 was carried out using CrysAlisPro, Oxford Diffraction Ltd. The structures were solved by direct method and refined by the full-matrix least-squares method against F^2 using SHELX-2018/3.[4] Non-hydrogen atoms were anisotropically refined. Positions of hydrogen atoms were included into refinement in a riding model. Crystal structure of **3** contains four independent solvent $C_6H_4Cl_2$ molecules. Three of them are ordered whereas the fourth molecule is strongly disordered. This molecule was masked by standard SQUUZE procedure. 340 electrons were found in a volume of 1388 $Å^3$ in 5 voids per unit cell. This is consistent with the presence of one additional $[C_6H_4Cl_2]$ molecule per asymmetric unit cell (totally four molecules were found). There is disorder of the $Os_3(CO)_{10}Cl$ cluster in **5**. The $Os(CO)_3$ fragment which is involved in the formation of the Os-Sn bond at such disorder is ordered but disorder is observed for two osmium atoms with surrounding ligands which do not participate in the Os-Sn bonding (the occupancy factors for disordered cluster are 0.8887(6)/0.1113(6)). Crystal structure of **6** contains only half independent $Cp^*_2Cr^+$ cation per one independent $\{Ir_4(CO)_{11}\cdot Sn^{II}(Pc^{\bullet 3-})\}_2$ unit providing unusual $(Cp^*_2Cr^+)\{Ir_4(CO)_{11}\cdot Sn^{II}(Pc^{\bullet 3-})\}_2^-$ composition of **6**.

Table S1. Crystallographic data and some details of data collection and refinement for **1**-**3**.

Compound	**1**	**2**	**3**
Empirical formula	$C_{43}H_{16}Co_4N_8O_{11}Sn$	$C_{61}H_{52}N_{10}NaO_{17}Ru_3Sn$	$C_{134}H_{120}Cl_8CsKN_{20}O_{22}Ru_3Sn_2$
M_r [g·mol^{-1}]	1175.05	1642.01	3358.69
Crystal color and shape,	Dark black prism	Dark black block	Dark black plate
Crystal system	monoclinic	monoclinic	orthorhombic
Space group	*P* 2_1/n	*P* 2_1/n	*P* na2_1
a, Å	12.9161(1)	17.3563(8)	26.2701(4)
b, Å	30.5606(3)	14.6148(7)	22.9467(5)
c, Å	10.9495(1)	25.1980(12)	22.6093(3)
α, °	90	90	90
β, °	107.391(1)	96.146(1)	90
γ, °	90	90	90
V, Å^3	4124.45(7)	6355.0(5)	13629.2(4)
Z	4	4	4
ρ_{calc} [g/cm^3]	1.892	1.716	1.637
μ [mm^{-1}]	2.247	1.173	1.213
F(000)	2304	3268	6728
T [K]	110(2)	293(2)	101(2)
2Θ, °	56.560	60.434	59.320
Reflns measured	45931	69976	121049
Unique reflns	9908	17737	29927
Params/Restraints	604/242	838/0	1576/1575
Reflns [F_o>2σ(F_o)]	8775	14674	22777
R_1 [F_o>2σ(F_o)]/wR_2 (all)	0.0223/0.0550	0.0368/0.0961	0.0882/0.2455
G.O.F	1.041	1.168	1.038
CCDC number	2115713	2115714	2115717

Table S2. Crystallographic data and some details of data collection and refinement for **4-6**.

Compound	**4**	**5**	**6**
Empirical formula	$C_{69}H_{50}Cl_2CrN_8O_{11}Ru_3Sn$	$C_{68}H_{50}Cl_3CrN_8O_{10}Os_3Sn$	$C_{53}H_{31}Cr_{0.50}Ir_4N_8O_{11}Sn$
M_r [g·mol^{-1}]	1711.97	1986.80	1869.35
Crystal color and shape,	Dark black prism	Dark black block	Dark black block
Crystal system	Monoclinic	monoclinic	
Space group	$P\ 2_1/n$	$P\ 2_1/n$	
a, Å	16.7801(1)	16.8961(4)	23.9498(5)
b, Å	20.0593(1)	20.0969(4)	15.1713(2)
c, Å	19.7671(1)	19.6999(4)	14.5364(4)
α, °	90	90	90
β, °	94.8720(10)	96.102(2)	97.584(2)
γ, °	90	90	90
V, Å^3	6629.51(6)	6651.4(2)	5235.6(2)
Z	4	4	4
ρ_{calc} [g/cm^3]	1.715	1.984	2.372
μ [mm^{-1}]	1.346	6.424	10.768
F(000)	3392	3788	3452
T [K]	120(2)	130(2)	130(2)
2Θ, °	70.500	52.744	65.814
Reflns measured	68094	90186	32472
Unique reflns	28227	13587	16896
Params/Restraints	866/0	819/0	705/367
Reflns [F_o>2σ(F_o)]	23076	12022	14494
R_1 [F_o>2σ(F_o)]/wR_2 (all)	0.0267/0.0603	0.0448/0.1130	0.0568/0.1376
G.O.F	1.046	1.031	1.096
CCDC number	2115715	2115716	2115712

Table S3. IR spectra of starting compounds and complexes **1-3**.

Components	$Sn^{II}(Pc^{2-})$	$Co_4(CO)_{12}$	$\{(Co_4(CO)_{11}\cdot Sn^{II}(Pc^{2-})\}$ (**1**)	Cryptand [2.2.2]	$Ru_3(CO)_{12}$	$\{Cryptand(Na^+)\}\cdot\{Ru_3(CO)_{11}\cdot Sn^{II}(Pc^{\bullet 3-})\}^-$ (**2**)	$\{Cryptand(M^+)\}_2\{Ru_3(CO)_{10}\cdot[Sn^{II}(Pc^{\bullet 3-})]_2\}^{2-}\cdot 4C_6H_4Cl_2$ (**3**)
$Sn^{II}(Pc^{2-})$	435w		-			440w*	440w
	498w		506w*			501w	502w
	725m		725s			712m	713s
	745m		750m			747m*	748m*
	768m		775m			765w	763m
	819w		825w			823w	822w
	872w		876w			-	-
	887m		892w			881w	889w
	948w		956w			950w	944m*
	1059s		-			-	1064m*
	1072s		1078m			1088s	-
	1114s		1121s			1115s*	1112vs
	1156w		1164w			1165w	1164w
	1283m		1289w			1263w	1260w
	1329s		1333s			1328m*	1330m*
	1407w		1420w			1421w	1420m
	1454w		1460w			1461m*	1464m*
	1486s		1478w			1497w*	1496w*
	3049w		3057w			3057w	3051w
$Cation^+$				476w		481w	-
				528w		-	-
				581w		567s*	569m*
				735m		747m*	748m*
				922m		928w	915w
				948w		-	944m*
				982m		-	-
				1038w		1038m	1033w*
				1071m		1072m	1064m*
				1100s		1103s	-
				1127s		1115s*	1112vs*
				1213w		-	-
				1295m		1301w	1298m
				1329m		1328m*	1330m*
				1360s		1356w	1353w
				1446m		-	-
				1462m		1461m*	1464m*
				1490w		1497w*	1496w*
				2790w		-	2813w
				2877w		2922w	2876m
				2943w		2967w	2956w
Transition metal cluster		422w	-		448w	440w*	440w
		482w	484w		466w	465w	463w
		510w	506w*		546m	-	-
		527w	530w		576m	567s	569m*
		545w	544w		592m	-	591w
		801w	798w		1997s	1988s 2000s	1963vs 1997vs
		1020w	1020w		2023s	2031s	2029m
		1099w	-		2059s	2080m	2193m
		1852s	1822m 1832m				
		2026s	1974m 1990m				
		2054s	2020s 2038s				
$C_6H_4Cl_2$			2076s				658w
							1033w*
							-

*- bands coincide; w – weak intensity, m –middle intensity, s – strong intensity; vs- very strong

Table S4. IR spectra of starting compounds and coordination complexes **4** and **5**.

Components	$Sn^{II}(Pc^{2-})$	Cp^*_2Cr	$Ru_3(CO)_{12}$	$\{Cp^*_2Cr^+\}\cdot\{Ru_3(CO)_{11}\cdot Sn^{II}(Pc^{\bullet 3-})\}^-\cdot C_6H_4Cl_2$ (**4**)	$Os_3(CO)_{12}$	$\{Cp^*_2Cr^+\}\cdot\{Ru_3(CO)_{10}Cl\cdot Sn^{II}(Pc^{\bullet 3-})\}^-\cdot C_6H_4Cl_2$ (**5**)
$Sn^{II}(Pc^{2-})$	435w			434w		434w
	498w			500w		494m*
	725m			716s		713s
	745m			745m		748s
	768m			763s		764s
	819w			825w		826w
	872w			-		-
	887m			884w		885w
	948w			948w		948w
	1059s			-		-
	1072s			1082w*		1084m*
	1114s			1113s		1113s
	1156w			1164m		1164m
	1283m			-		-
	1329s			1327m		1327m
	1407w			1421w*		1418m*
	1454w			1457w*		1455w*
	1486s			1470w		1472w
	3049w			3057w		3057w
$Cation^+$		419w		-		-
		585w		566s*		569m
		1022s		1021w		1022w
		1068w		1082w*		1084m*
		1262w		-		-
		1316s		1303w		1305w
		1375s		1383m		1382m
		1414w		-		-
		1423m		1421w*		1418m*
		1448w		1433w		1435w
		1634m		-		-
		2852w		2852w		2855w
		2899w		2920w		2919w
		2955w		-		
Transition metal cluster			-	-	410w	406w
			448w	450w	431w	427w
			466w	461w	463w	453w
			-		496w	494m*
			546m	-	563w	-
			576m	566s*	584m	591s
			592m	-	604m	618w
			1997s	1978s 1990s	1984s 1994s	1963s 2006s
			2023s	2001s 2012s	2016s 2028s 2040s	2040s 2063s
			2059s	2033s 2082m	2060s 2068s	2100s
Solvent $C_6H_4Cl_2$				658w		657w
				1033w*		1034w
				1457w*		1455w*

* - bands are coincided; w – weak intensity, m –middle intensity, s – strong intensity

IR spectra of starting compounds and coordination complexes with clusters.

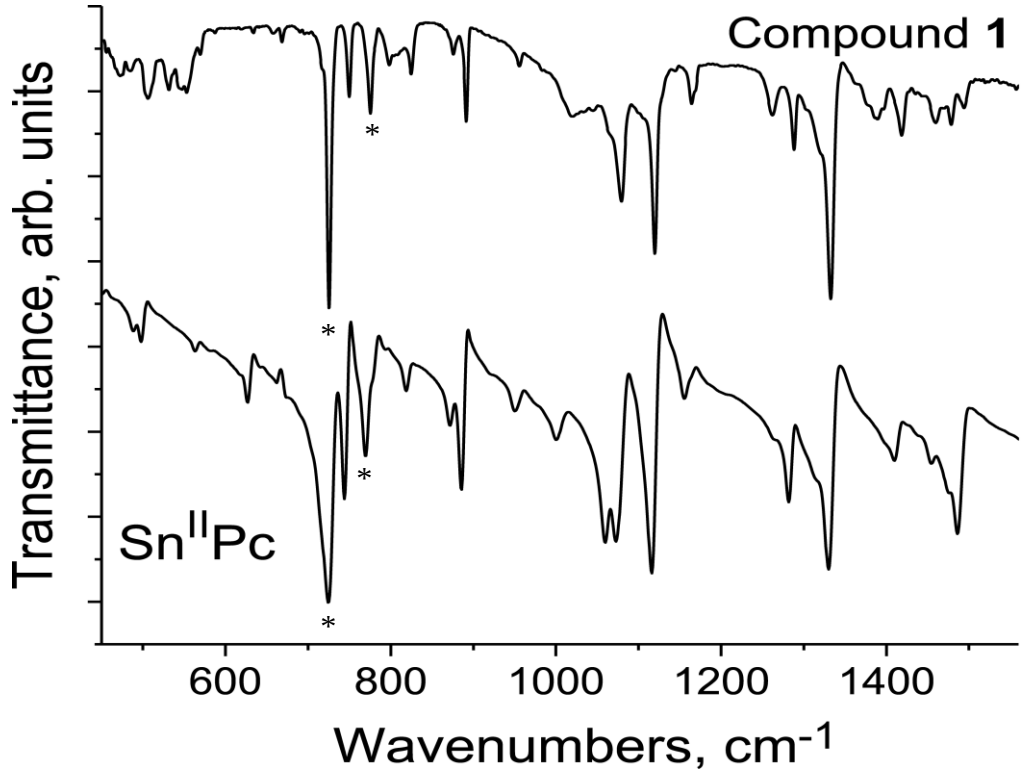

Figure S1. IR spectra of starting tin(II) phthalocyanine $[Sn^{II}(Pc^{2-})]^0$ and coordination complex $\{Co_4(CO)_{11}\cdot Sn^{II}(Pc^{2-})\}$ (**1**) in KBr pellets. Pellet for **1** was prepared in anaerobic conditions.

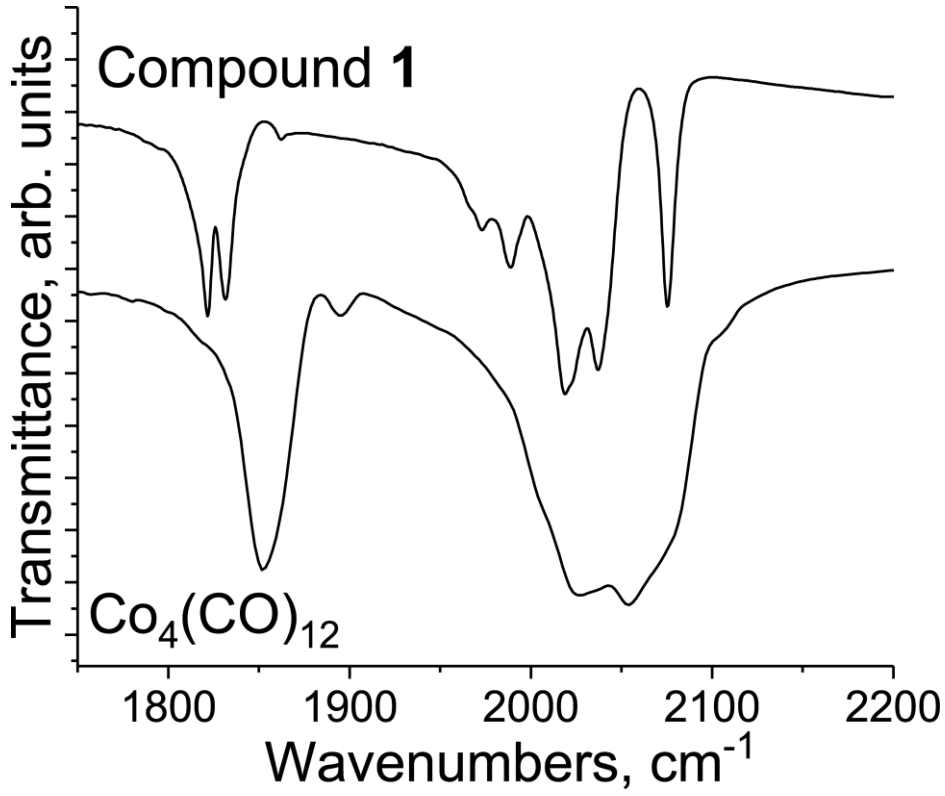

Figure S2. IR spectra in the range of the C≡O vibrations for starting $Co_4(CO)_{12}$ cluster and coordination complex $\{Co_4(CO)_{11}\cdot Sn^{II}(Pc^{2-})\}$ (**1**) in KBr pellets prepared in anaerobic conditions.

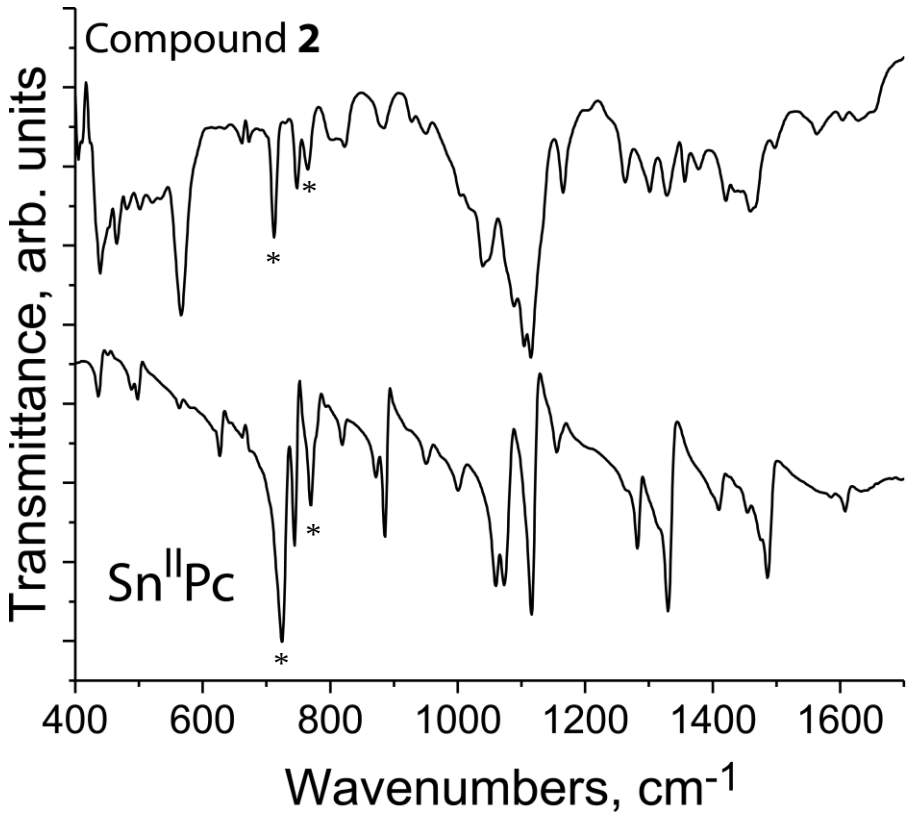

Figure S3. IR spectra of starting tin(II) phthalocyanine $[Sn^{II}(Pc^{2-})]^0$ and coordination complex $\{Cryptand(Na^+)\}\{Ru_3(CO)_{11}\cdot Sn^{II}(Pc^{\bullet 3-})\}^-$ (**2**) in KBr pellets. Pellet for **2** was prepared in anaerobic conditions.

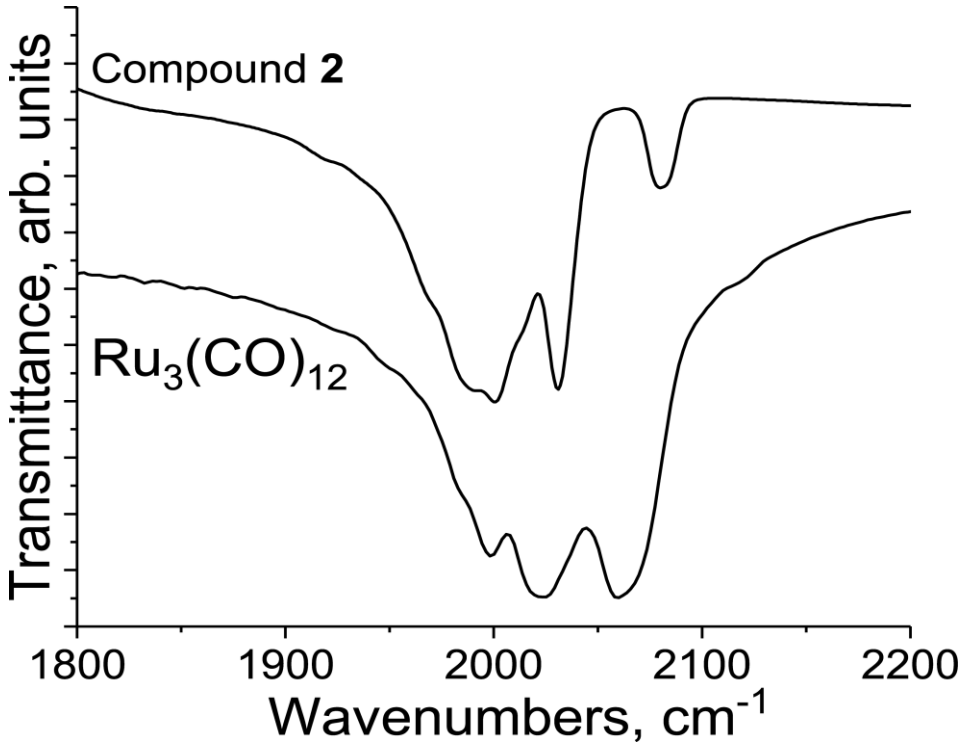

Figure S4. IR spectra in the range of the C≡O vibrations for starting $Ru_3(CO)_{12}$ cluster and coordination complex $\{Cryptand(Na^+)\}\{Ru_3(CO)_{11}\cdot Sn^{II}(Pc^{\bullet 3-})\}^-$ (**2**) in KBr pellets prepared in anaerobic conditions.

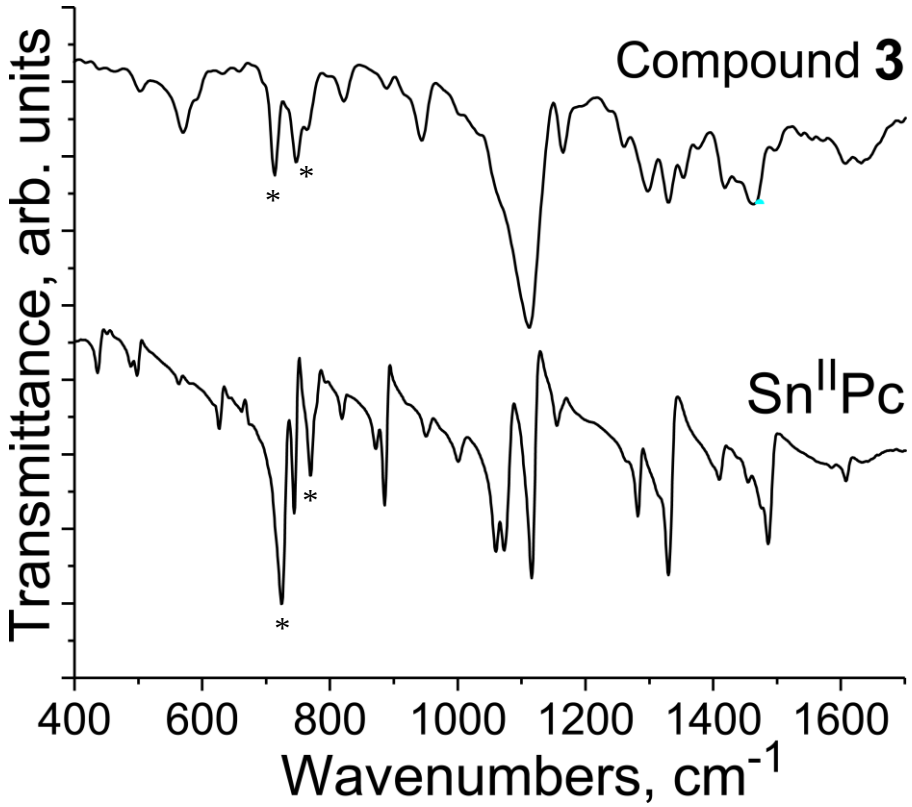

Figure S5. IR spectra of starting tin(II) phthalocyanine $[Sn^{II}(Pc^{2-})]^0$ and coordination complex $\{Cryptand(M^+)\}_2\{Ru_3(CO)_{10}\cdot[Sn^{II}(Pc^{\bullet 3-})]_2\}^{2-}\cdot 4C_6H_4Cl_2$ (**3**) in KBr pellets. Pellet for **3** was prepared in anaerobic conditions.

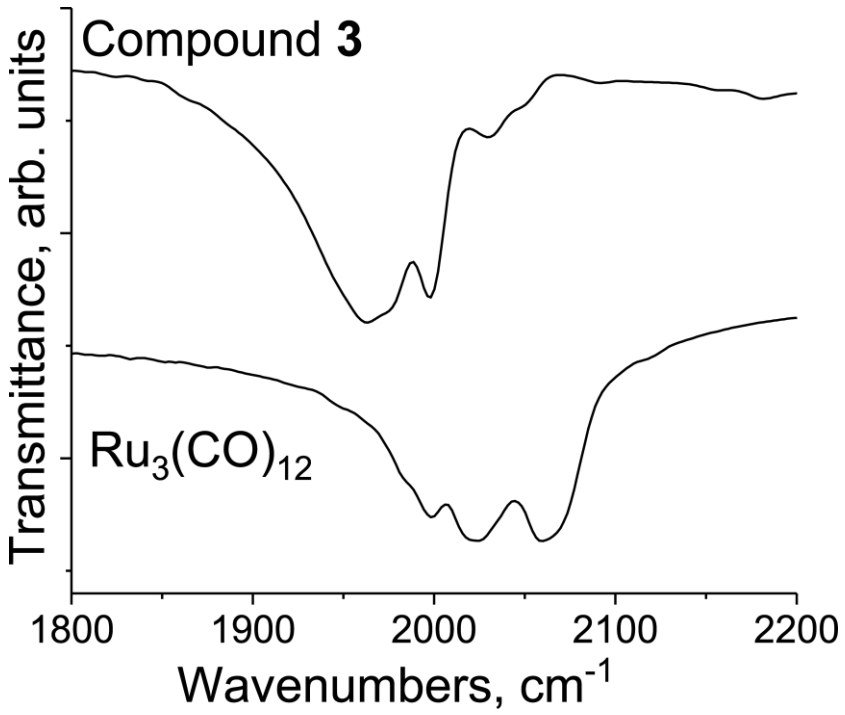

Figure S6. IR spectra in the range of the C≡O vibrations for starting $Ru_3(CO)_{12}$ cluster and coordination complex $\{Cryptand(M^+)\}_2\{Ru_3(CO)_{10}\cdot[Sn^{II}(Pc^{\bullet 3-})]_2\}^{2-}\cdot 4C_6H_4Cl_2$ (**3**) in KBr pellets prepared in anaerobic conditions.

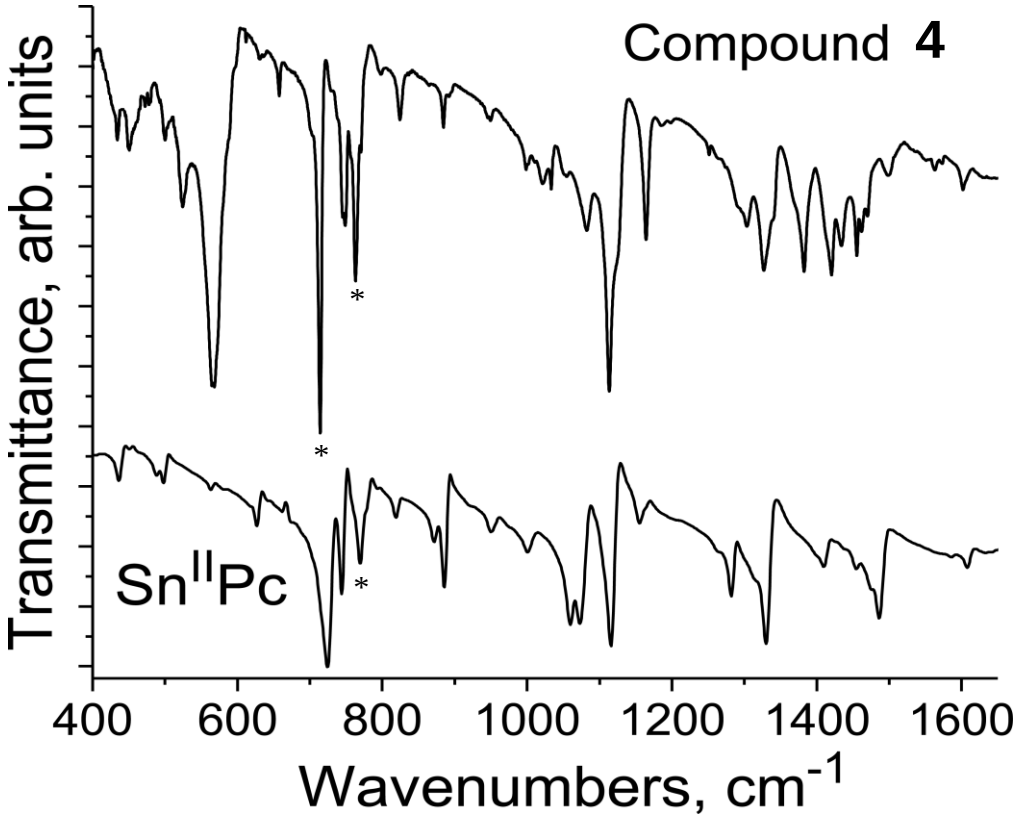

Figure S7. IR spectra of starting tin(II) phthalocyanine $[Sn^{II}(Pc^{2-})]^0$ and coordination complex $\{Cp^*_2Cr^+\}\{Ru_3(CO)_{11}\cdot Sn^{II}(Pc^{\bullet 3-})\}^-\cdot C_6H_4Cl_2$ (**4**) in KBr pellets. Pellet for **4** was prepared in anaerobic conditions.

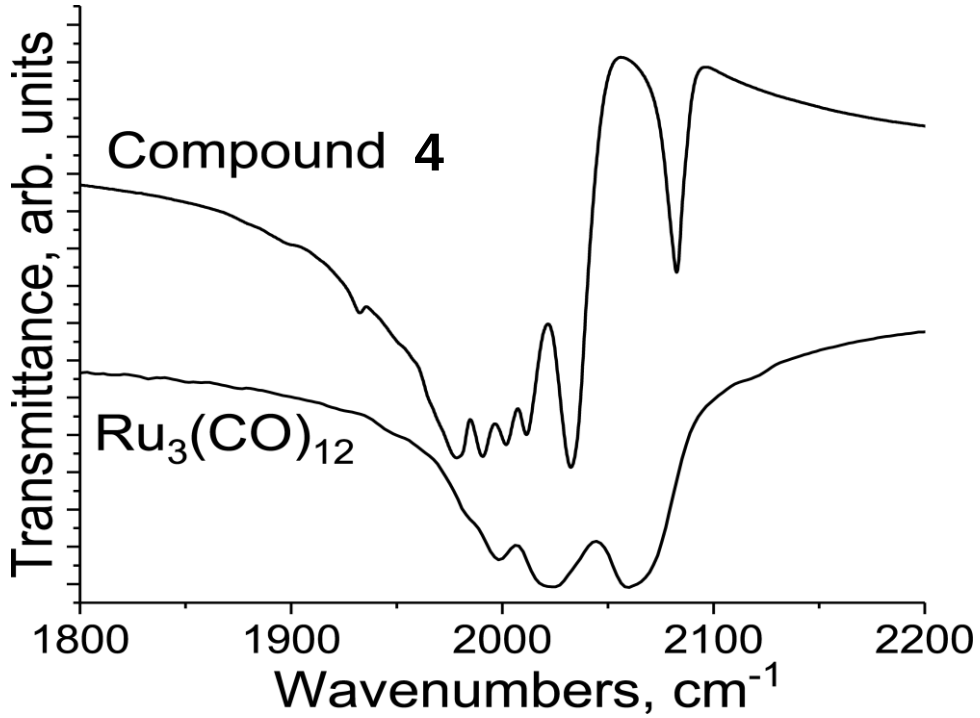

Figure S8. IR spectra in the range of the C≡O vibrations for starting $Ru_3(CO)_{12}$ cluster and coordination complex $\{Cp^*_2Cr^+\}\{Ru_3(CO)_{11}\cdot Sn^{II}(Pc^{\bullet 3-})\}^-\cdot C_6H_4Cl_2$ (**4**) in KBr pellets prepared in anaerobic conditions.

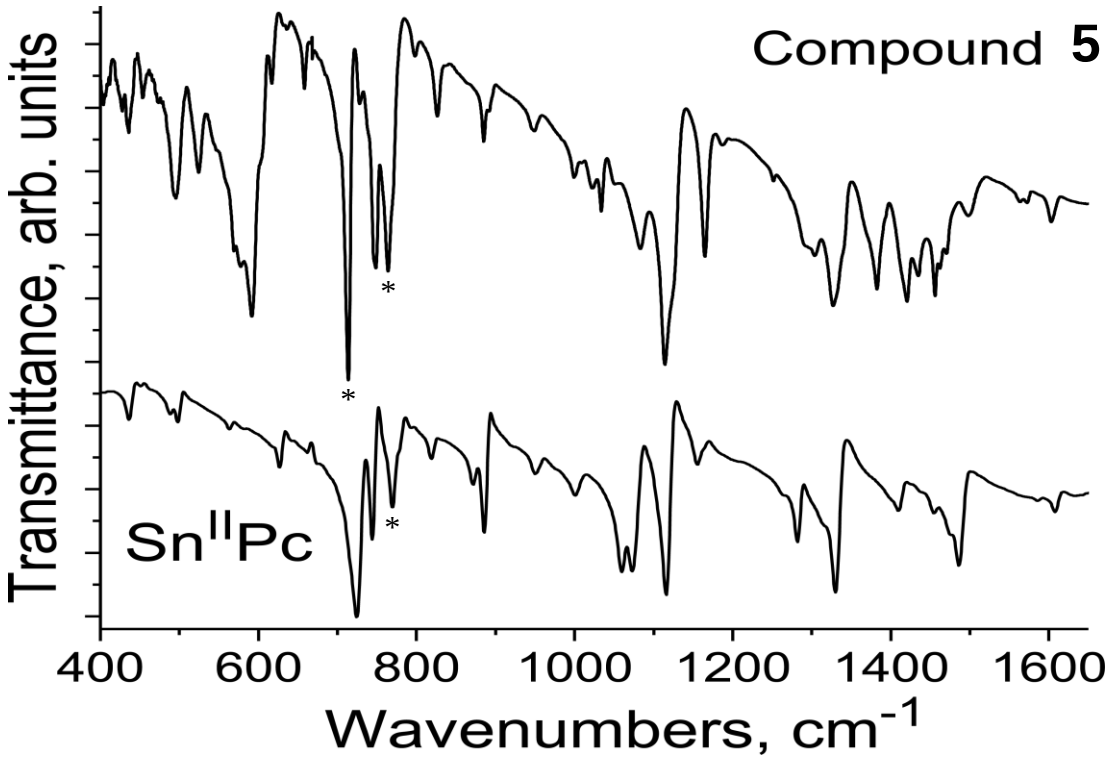

Figure S9. IR spectra of starting tin(II) phthalocyanine $[Sn^{II}(Pc^{2-})]^0$ and coordination complex $\{Cp^*_2Cr^+\}\cdot\{Os_3(CO)_{10}Cl\cdot Sn^{II}(Pc^{\bullet 3-})\}^-\cdot C_6H_4Cl_2$ (**5**) in KBr pellets. Pellet for **5** was prepared in anaerobic conditions.

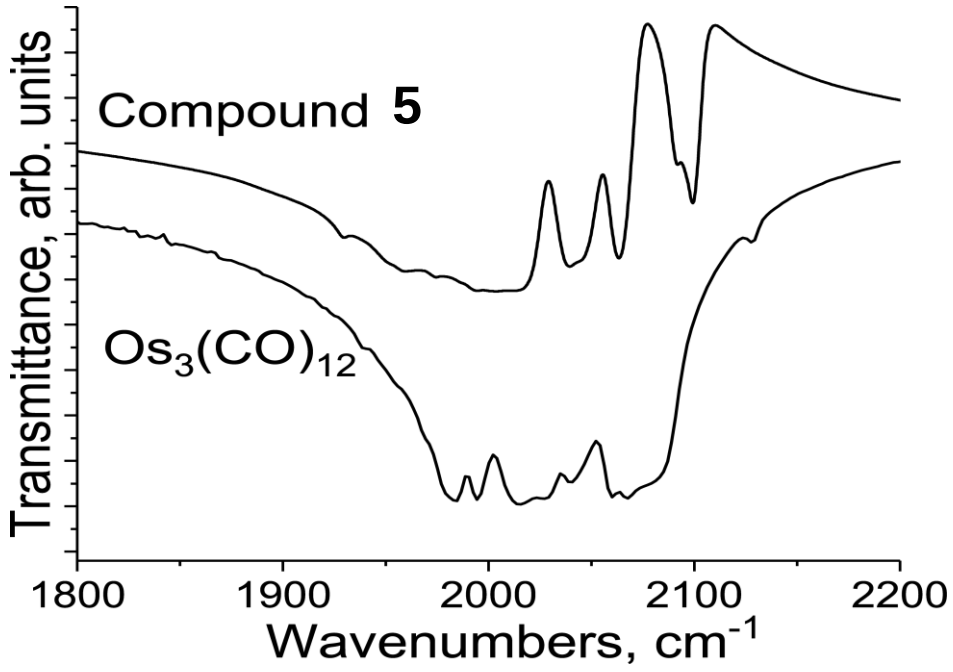

Figure S10. IR spectra in the range of the C≡O vibrations for starting $Os_3(CO)_{12}$ cluster and coordination complex $(Cp^*_2Cr^+)\cdot\{Os_3(CO)_{10}Cl\cdot Sn^{II}(Pc^{\bullet 3-})\}^-\cdot C_6H_4Cl_2$ (**5**) in KBr pellets prepared in anaerobic conditions.

Crystal structures.

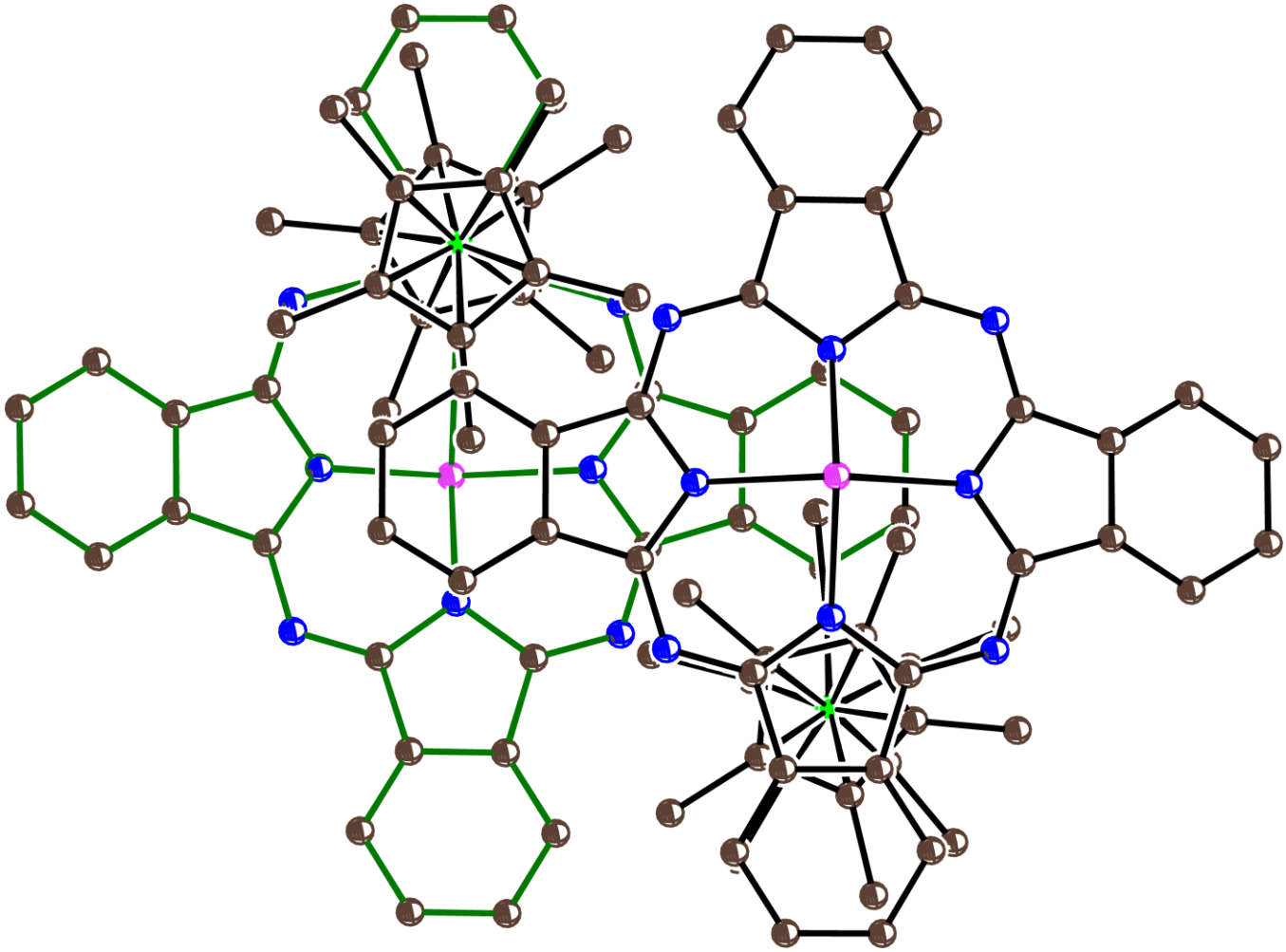

Figure S11. View on one $(Cp^*_2Cr^+)_2\{Ru_3(CO)_{11}\cdot Sn^{II}(Pc^{\bullet 3-})\}^-_2$ unit in the crystal structure of $\{Cp^*_2Cr^+)\}\{Ru_3(CO)_{11}\cdot Sn^{II}(Pc^{\bullet 3-})\}^-\cdot C_6H_4Cl_2$ (**4**) along the $Cp^*_2Cr^+$ cations. $Ru_3(CO)_{11}$ clusters are not shown for clarity. Bonds of far $\{Sn^{II}(Pc^{\bullet 3-})\}^-$ anion within the unit are shown by dark green color.

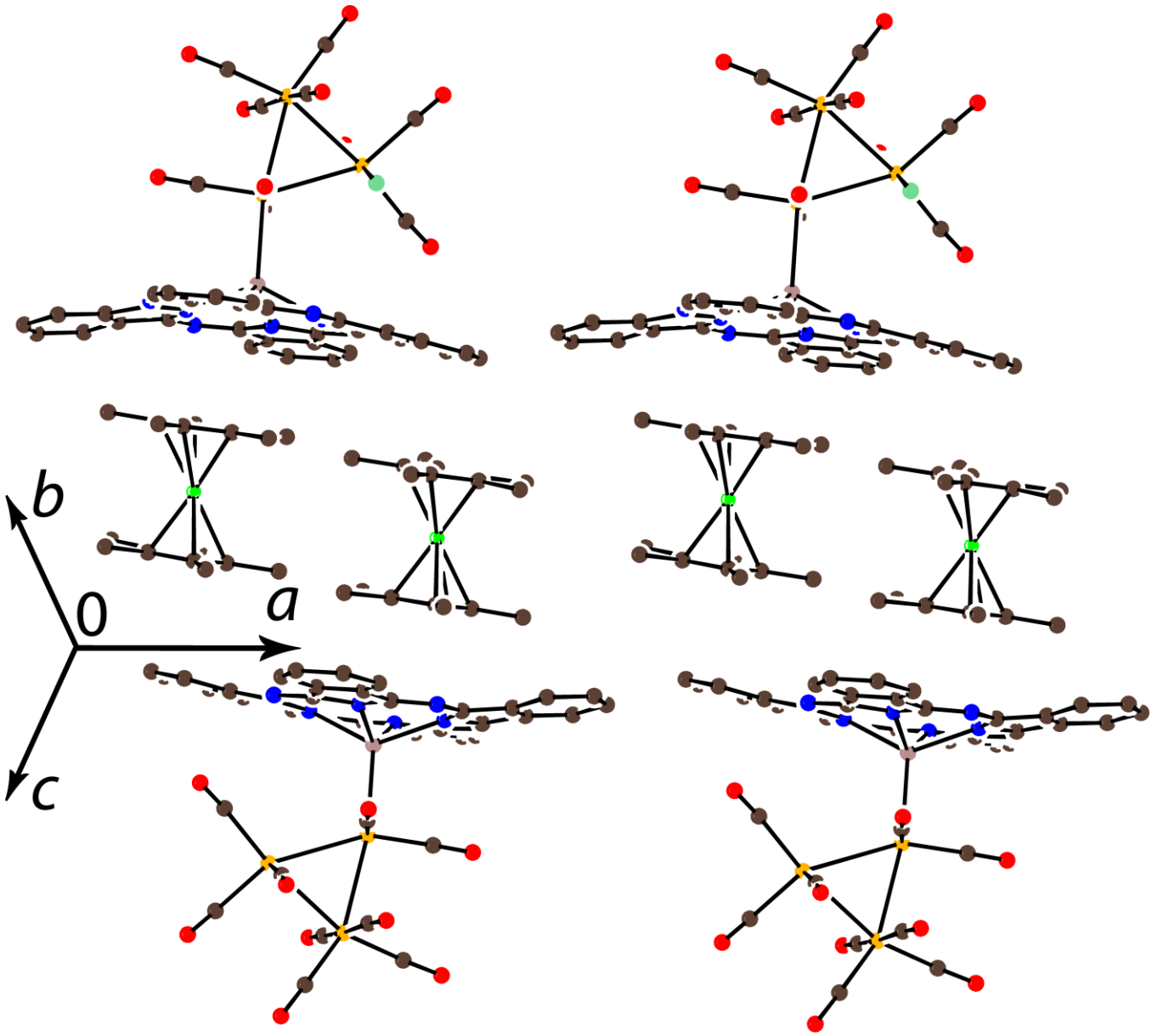

Figure S12. View on the crystal structure of complex $\{Cp^*_2Cr^+)\}\{Os_3(CO)_{10}Cl\cdot Sn^{II}(Pc^{\bullet 3-})\}^-\cdot C_6H_4Cl_2$ (**5**). Solvent molecules are not shown. Only one orientation of the $Os_3(CO)_{10}Cl$ cluster is shown.

UV-visible-NIR spectra

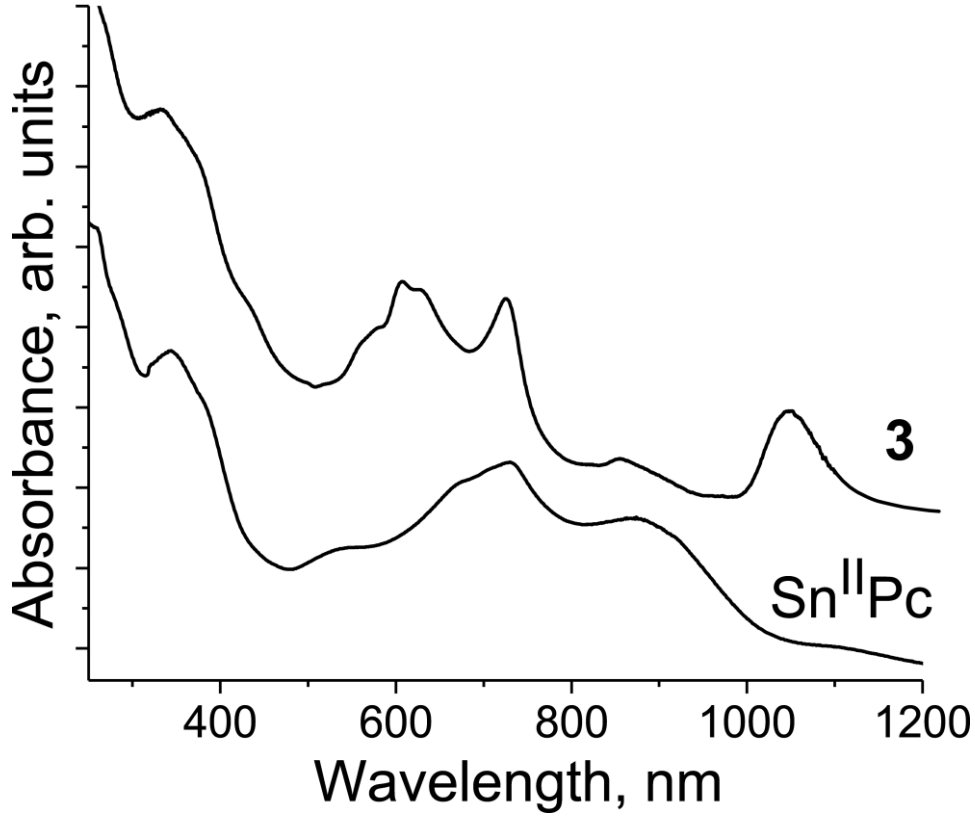

Figure S13. UV-visible-NIR spectra of pristine $Sn^{II}(Pc^{2-})$ and complex $\{Cryptand(M^{+})\}_2\{Ru_3(CO)_{10}\cdot[Sn^{II}(Pc^{\bullet 3-})]_2\}^{2-}\cdot 4C_6H_4Cl_2$ (**3**) (M = K, Cs) containing radical trianion $Pc^{\bullet 3-}$ macrocycles.

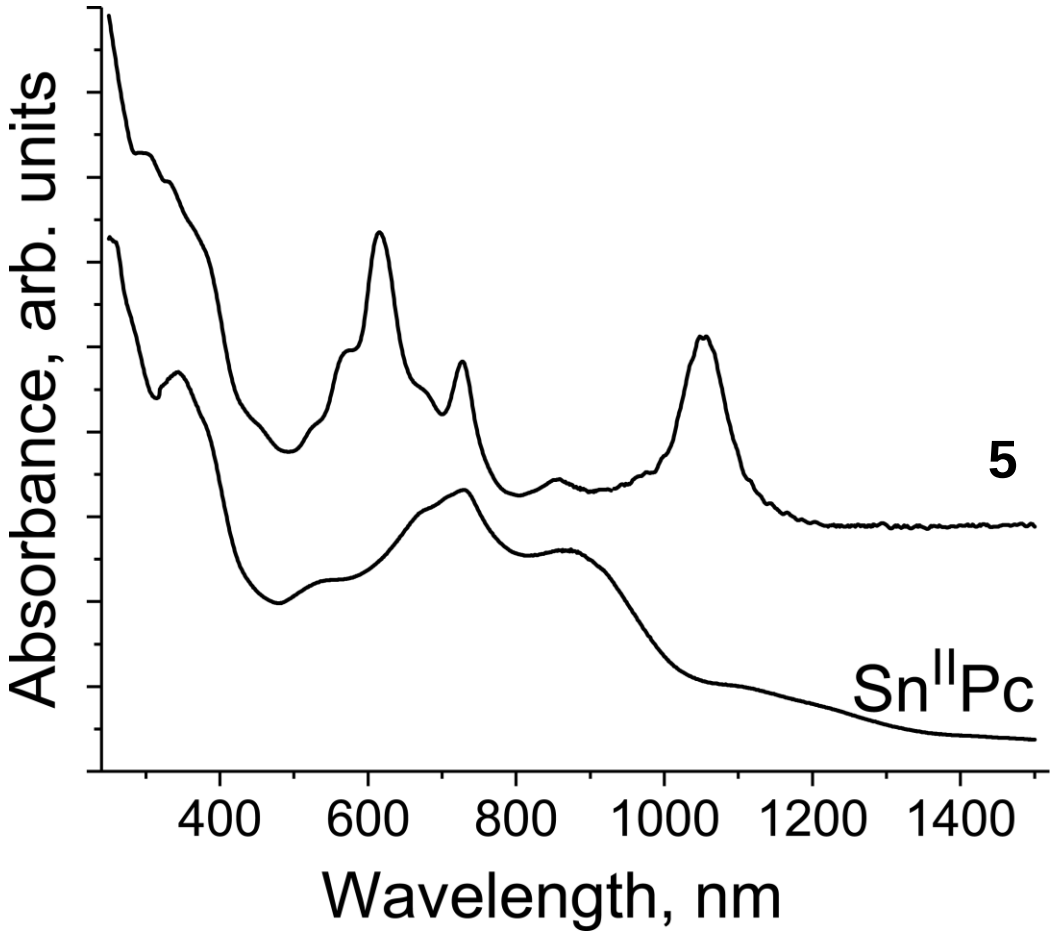

Figure S14. UV-visible-NIR spectra of pristine $Sn^{II}(Pc^{2-})$ and complex $\{Cp^*_2Cr^+)\}\{Os_3(CO)_{10}Cl\cdot Sn^{II}(Pc^{\bullet 3-})\}^-\cdot C_6H_4Cl_2$ (**5**) containing radical trianion $Pc^{\bullet 3-}$ macrocycles.

Magnetic data

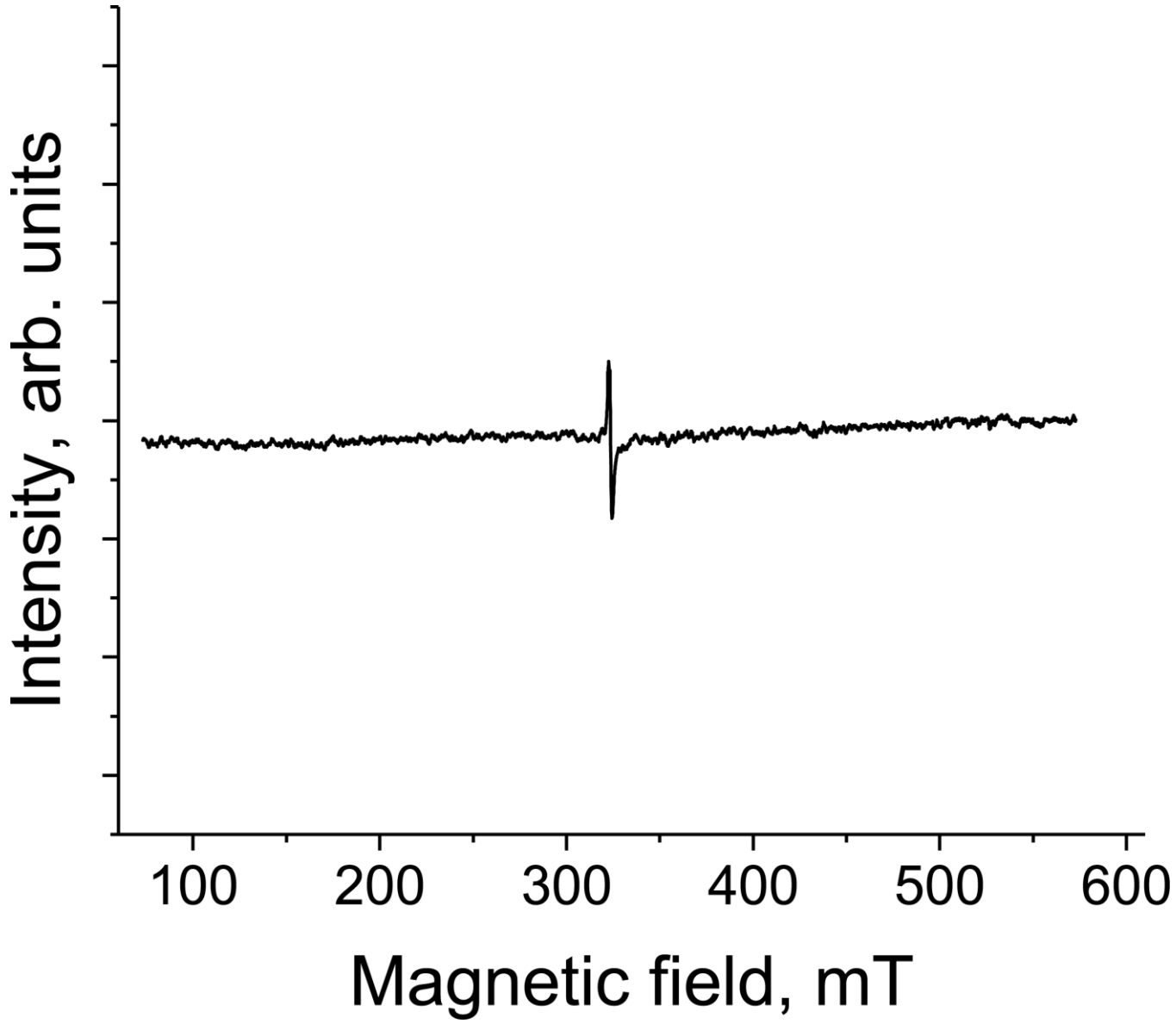

Figure S15. EPR spectrum of {($Co_4(CO)_{11}$·$Sn^{II}(Pc^{2-})$} (**1**) at 70 K and large amplification of the signal. Integral intensity of a weak signal at about 323 mT corresponds to less than 0.1% from the content of SnPc.

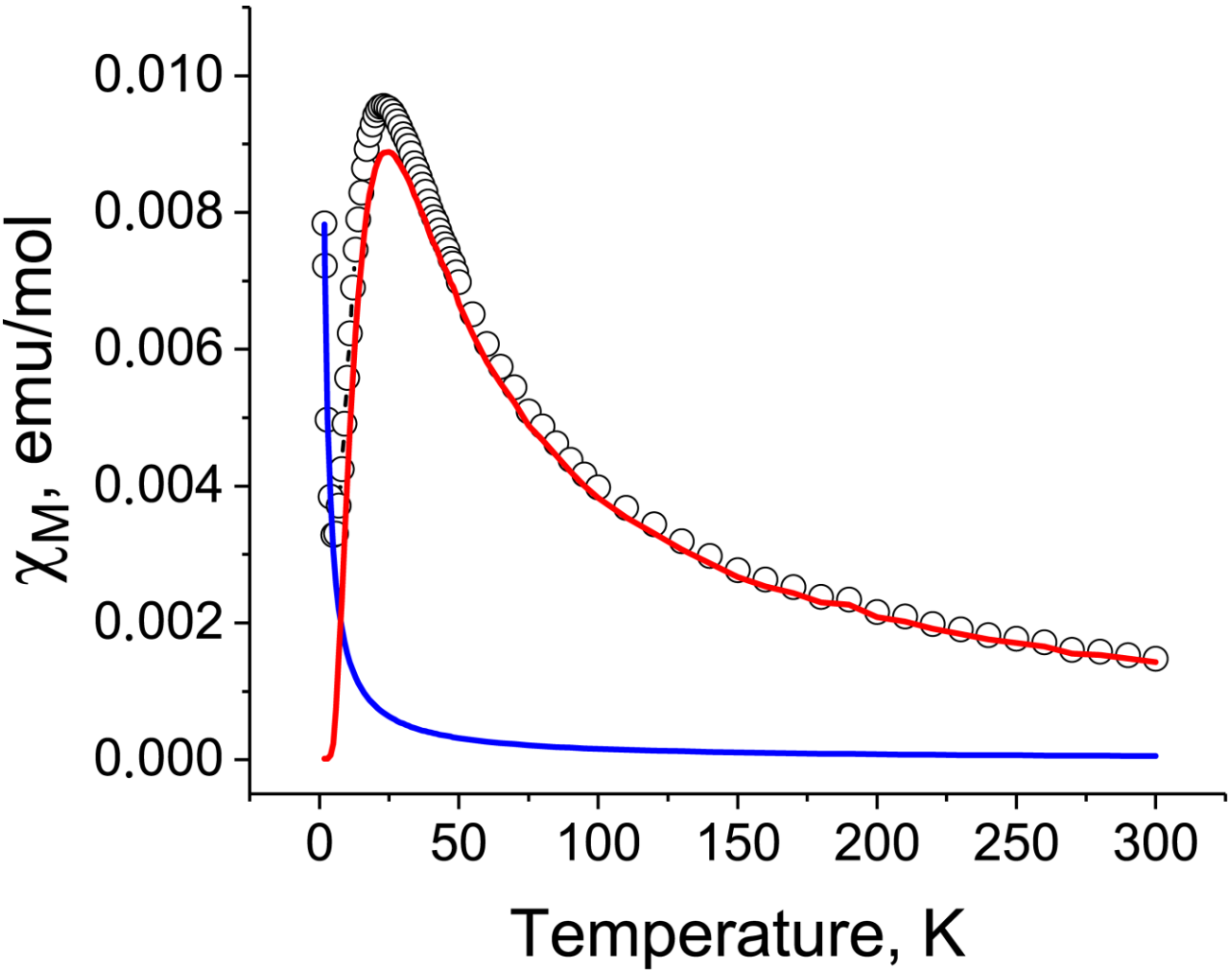

Figure S16. Experimental data of molar magnetic susceptibility of complex {Cryptand(Na^+)} {$Ru_3(CO)_{11}\cdot Sn^{II}(Pc^{\bullet 3-})\}^-$ (**2**) (open circles) and approximation of the data by two contributions: from Curie impurities with C = 0.0133 (3.6% of the S =1/2 spins from total amount of $\{Sn^{II}(Pc^{\bullet 3-})\}^-$, blue curve) and bulk sample (red curve).

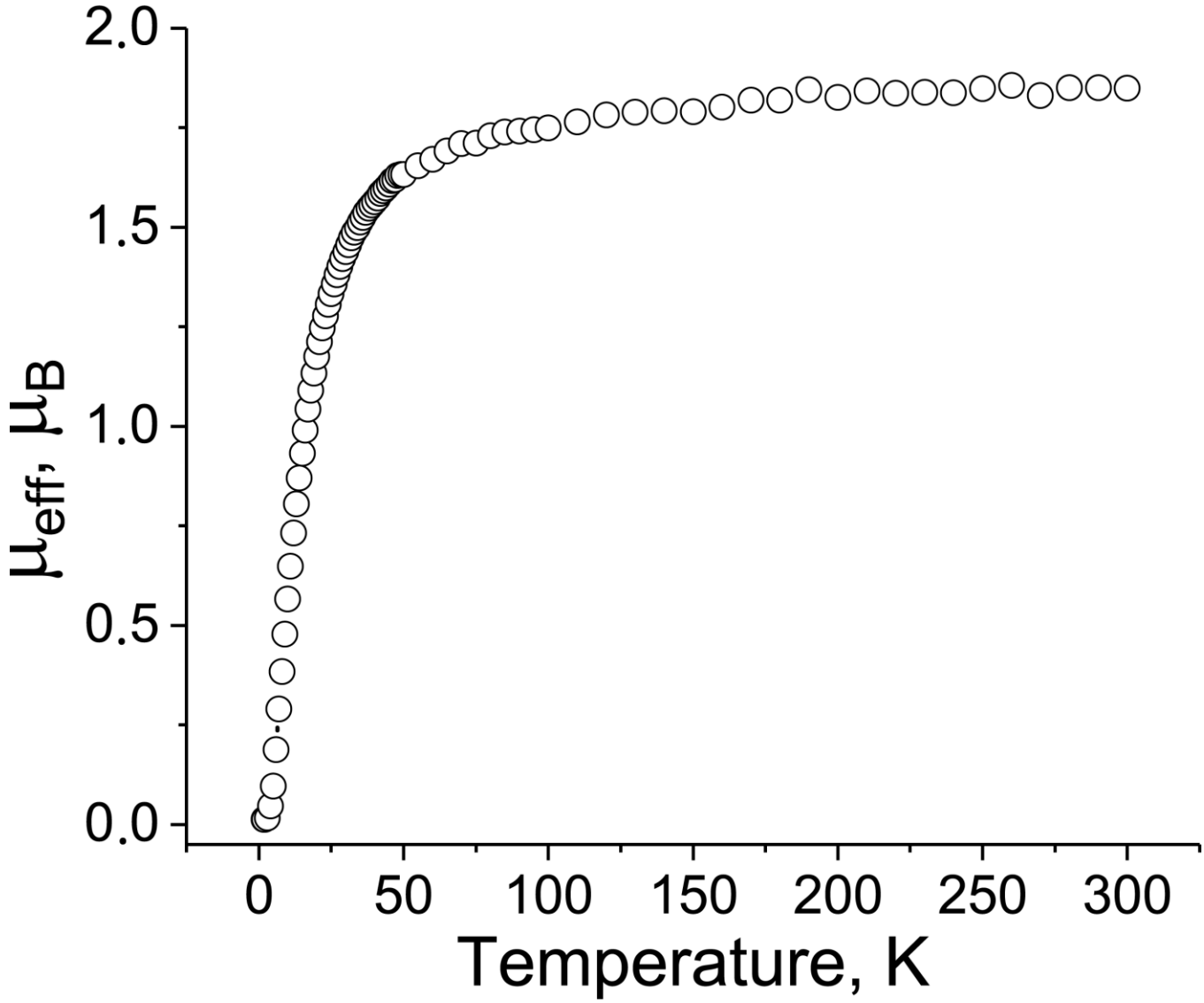

Figure S17. Temperature dependence of effective magnetic moment of complex {Cryptand(Na^+)}{$Ru_3(CO)_{11}\cdot Sn^{II}(Pc^{\bullet 3-})$}$^-$ (**2**) in the 1.9-300 K range.

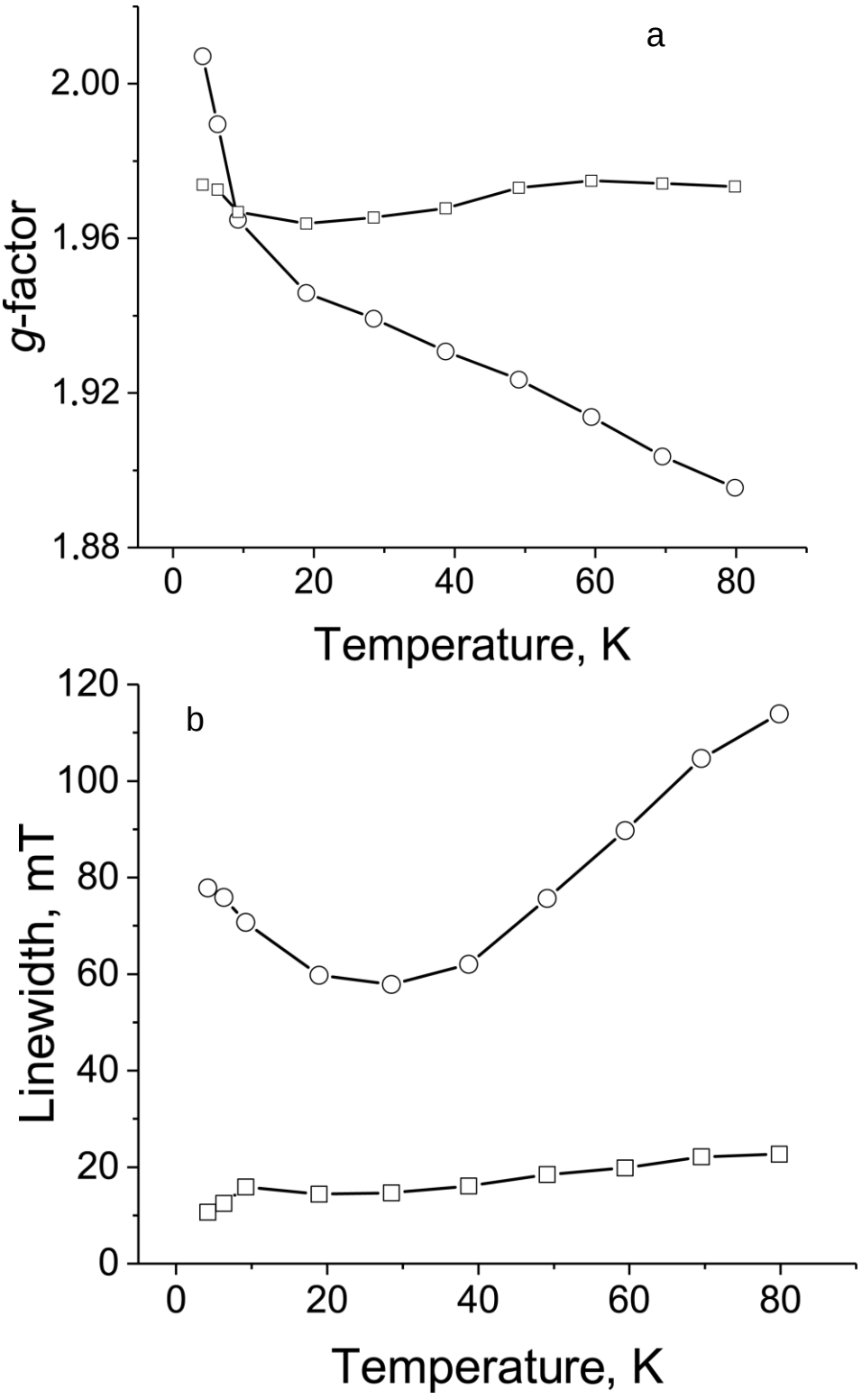

Fig. S18. Temperature dependencies of the parameter of broad EPR signal in **2** from 80 down to 4.2 K: (a) *g*-factor and (b) the linewidth.

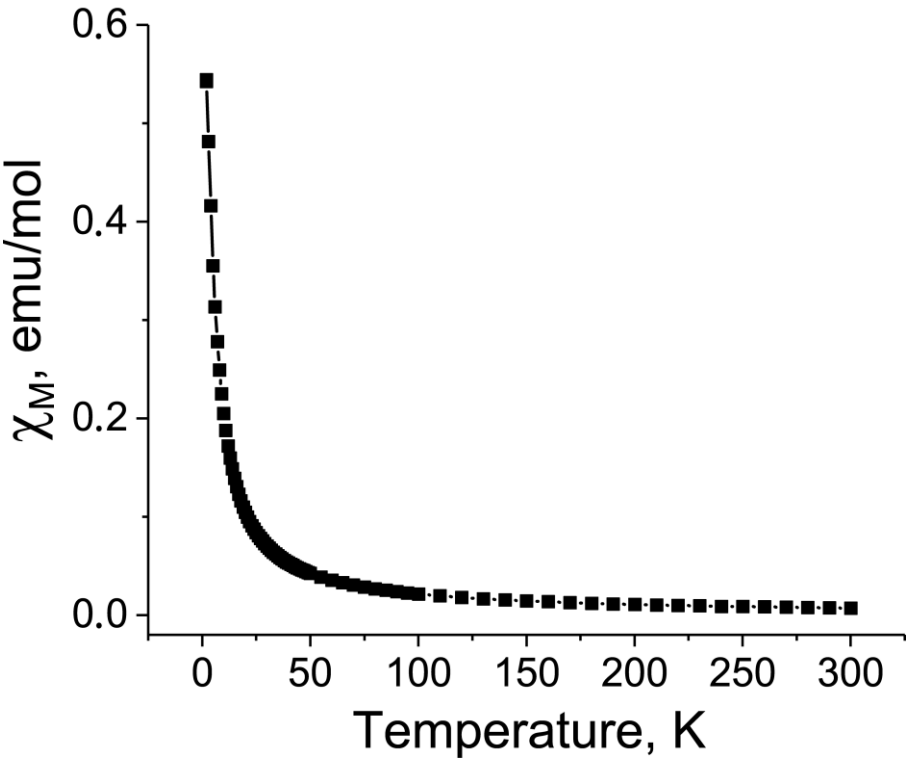

Figure S19. Temperature dependence of molar magnetic susceptibility of $\{Cp^*_2Cr^+)\}\{Ru_3(CO)_{11}\cdot Sn^{II}(Pc^{\bullet 3-})\}^-\cdot C_6H_4Cl_2$ (**4**).

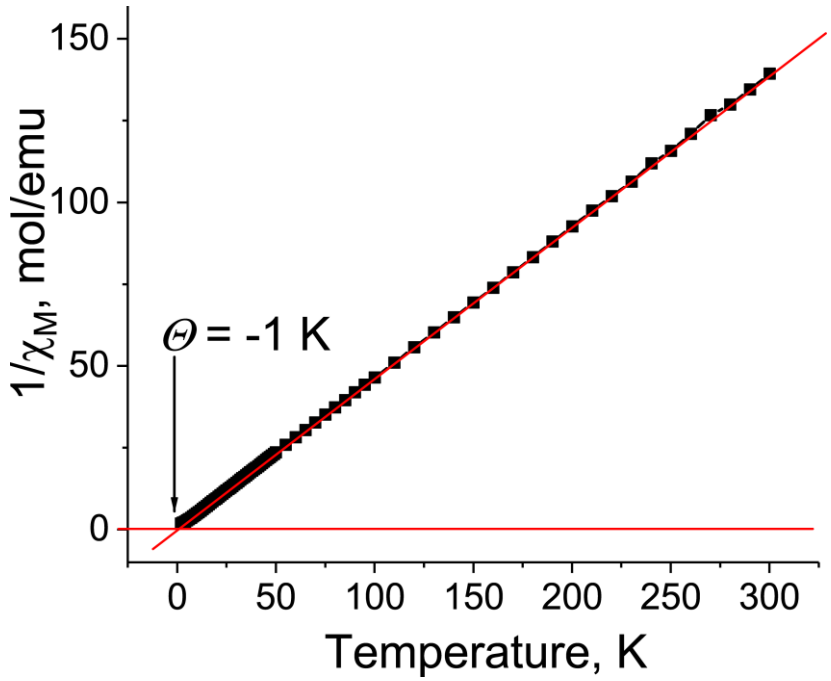

Figure S20. Temperature dependence of reciprocal molar magnetic susceptibility of $\{Cp^*_2Cr^+)\}\{Ru_3(CO)_{11}\cdot Sn^{II}(Pc^{\bullet 3-})\}^-\cdot C_6H_4Cl_2$ (**4**) which allows Weiss temperature to be determined as -1 K.

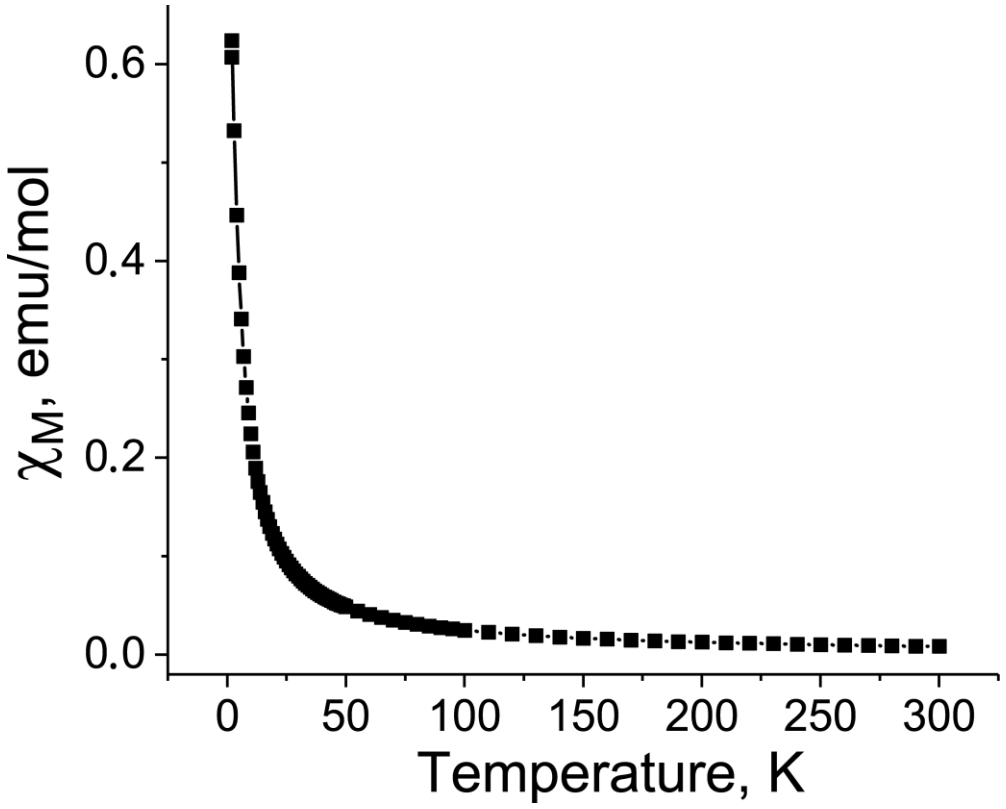

Figure S21. Temperature dependence of molar magnetic susceptibility of $\{Cp^*_2Cr^+\}\{Os_3(CO)_{10}Cl\cdot Sn^{II}(Pc^{\bullet 3-})\}^-\cdot C_6H_4Cl_2$ (**5**).

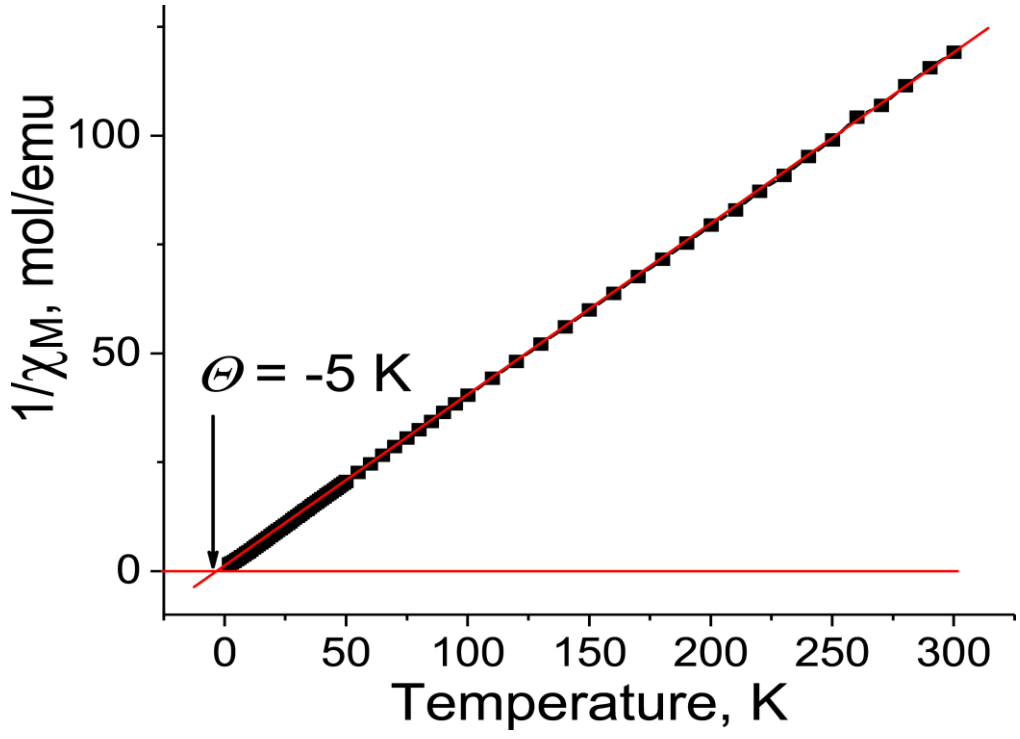

Figure S22. Temperature dependence of reciprocal molar magnetic susceptibility of $\{Cp^*_2Cr^+\}\{Os_3(CO)_{10}Cl\cdot Sn^{II}(Pc^{\bullet 3-})\}^-\cdot C_6H_4Cl_2$ (**5**) which allows Weiss temperature to be determined as -5 K.

Theoretical calculations.

Computational

DFT calculations based on the MN12-L[5], MN12-SX[6], and CAM-B3LYP-D3(BJ)[7] functionals were performed using the cc-pVTZ-PP,[8] cc-pVTZ,[9] and cc-pVDZ[10] basis sets for Sn, Co, and the other atoms, respectively. Partial geometry optimizations on the coordinates of only hydrogen atoms based on the X-ray structure were performed with "Opt = Tight" keyword. In the present calculations, "Int =SuperFineGrid" was specified, and stabilities of the wave functions were confirmed by specifying the "Stable = Opt" keyword. The subsequent natural bond orbital (NBO) analysis was performed using the NBO program.[11] The computations were performed with the Gaussian 09 program package.[12]

Table S5. Method, state, total and relative energy (E and ΔE), and $\langle S^2 \rangle$ value of $\{Co_4(CO)_{11}Sn^{II}(Pc^{2-})\}$ calculated at the MN12-L, MN12-SX, and CAM-B3LYP-D3(BJ)/cc-pVTZ-PP/cc-pVTZ/cc-pVDZ levels of theory.

Method	State	E / hartree	ΔE / K	$\langle S^2 \rangle$
UMN12-L	^{5}A	−8654.6306887	29049	6.061
UMN12-L	^{3}A	−8654.6803389	13371	2.023
RMN12-L	^{1}A	−8654.7226823	0	0
UMN12-L	^{1}A	−8654.7226823	0	0
UMN12-SX	^{5}A	−8655.8955931	21970	6.398
UMN12-SX	^{3}A	−8655.9284202	11604	2.916
RMN12-SX	^{1}A	−8655.9651682	0	0
UMN12-SX	^{1}A	−8655.9701447	−1571	0.903
UCAM-B3LYP-D3(BJ)	^{5}A	−8658.9100981	11230	6.801
UCAM-B3LYP-D3(BJ)	^{3}A	−8658.9404017	1661	3.576
RCAM-B3LYP-D3(BJ)	^{1}A	−8658.9456615	0	0
UCAM-B3LYP-D3(BJ)	^{1}A	−8658.9691797	−7426	1.589

Table S6. Natural charge and spin densities on Sn atom, Pc and $Co_4(CO)_{11}$ moieties in the ^1A, ^3A , and ^5A states of $\{Co_4(CO)_{11}\cdot Sn^{II}(Pc^{2-})\}$ calculated at the MN12-L, MN12-SX, and CAM-B3LYP-D3(BJ)/cc-pVTZ-PP/cc-pVTZ/cc-pVDZ levels of theory.

	^1A		^3A		^5A	
	charge	spin	charge	spin	charge	spin
MN12-L						
Sn	2.057	0	2.053	0.012	2.053	0.017
Pc	−1.036	0	−1.022	1.984	−1.025	1.993
$Co_4(CO)_{11}$	−1.022	0	−1.031	0.004	−1.027	1.991
MN12-SX						
Sn	2.061	−0.022	2.057	−0.014	2.063	−0.005
Pc	−1.079	−0.006	−1.065	1.983	−1.060	1.979
$Co_4(CO)_{11}$	−0.982	0.028	−0.992	0.031	−1.003	2.026
CAM-B3LYP-D3(BJ)						
Sn	2.005	−0.040	2.001	−0.031	1.996	−0.019
Pc	−1.053	−0.012	−1.038	1.979	−1.027	1.984
$Co_4(CO)_{11}$	−0.952	0.051	−0.964	0.053	−0.969	2.036

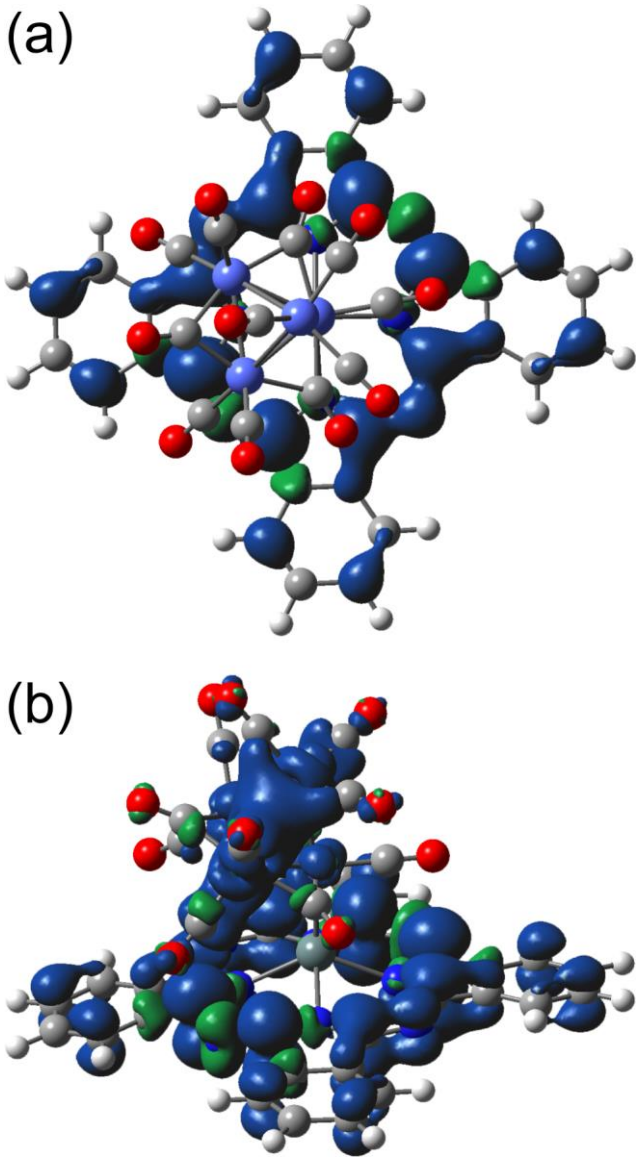

Figure S23. Spin density distributions of the (a) ^{3}A and (b) ^{5}A states in $\{Co_4(CO)_{11}\cdot Sn^{II}(Pc^{2-})\}$ calculated at the UMN12-L/cc-pVTZ-PP/cc-pVTZ/cc-pVDZ level of theory.

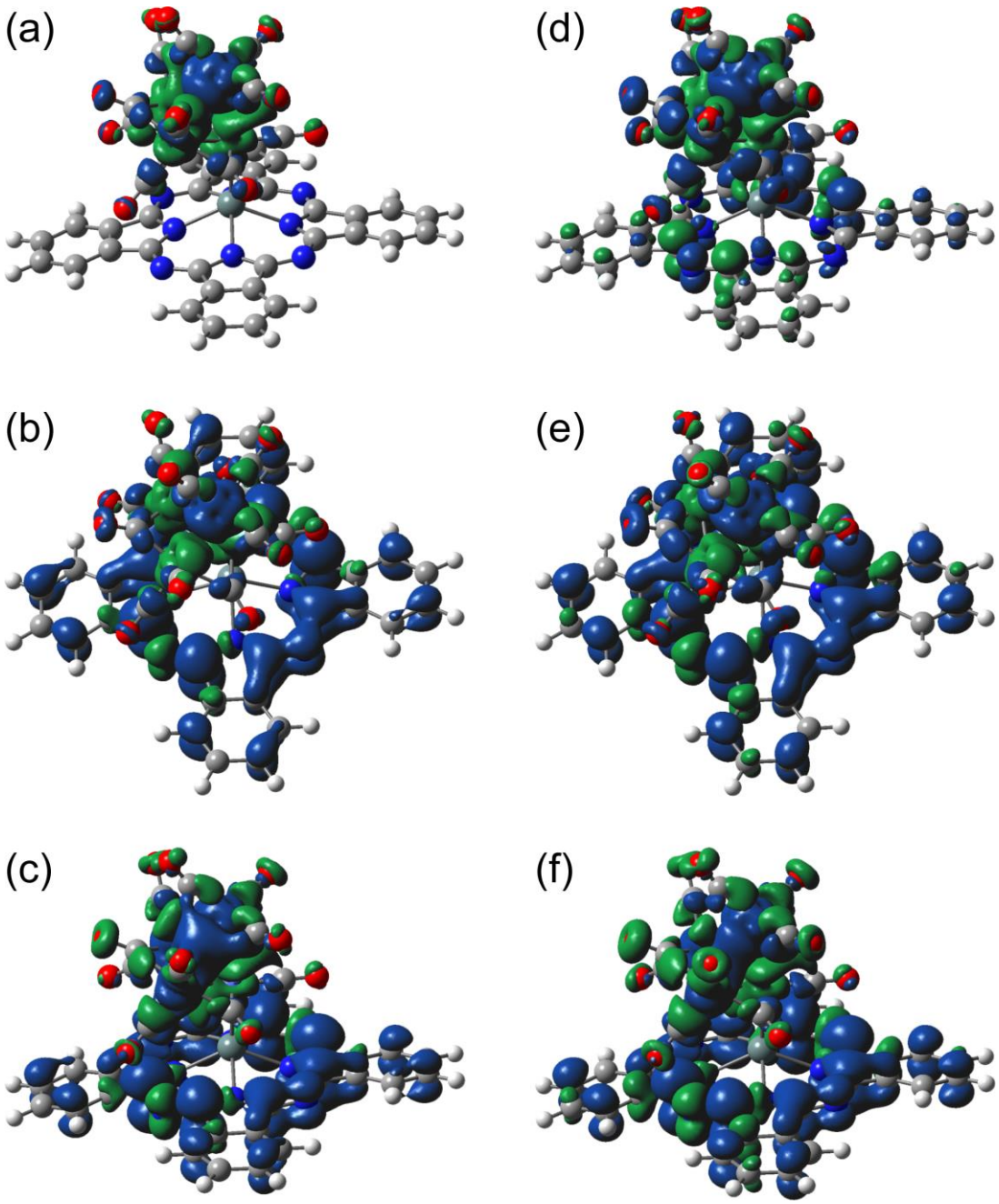

Figure S24. Spin density distributions in $\{Co_4(CO)_{11}\cdot Sn^{II}(Pc^{2-})\}$. The (a) ^1A, (b) ^3A, and (c) ^5A states calculated at the UMN12-SX/cc-pVTZ-PP/cc-pVTZ/cc-pVDZ level of theory. The (d) ^1A, (e) ^3A, and (f) ^5A states calculated at the UCAM-B3LYP-D3(BJ)/cc-pVTZ-PP/cc-pVTZ/cc-pVDZ level of theory.

References

1. D. V. Konarev, S. S. Khasanov, E. I. Yudanova, R. N. Lyubovskaya, *Eur. J. Inorg. Chem.*, 2011, 816-820.
2. D. V. Konarev, A. V. Kuzmin, S. S. Khasanov, A. F. Shestakov, A. L. Litvinov, P. A. Sobov, A. Otsuka, H. Yamochi, H. Kitagawa, R. N. Lyubovskaya, *Inorg. Chem.*, 2020, 59, 1169 – 1175.
3. G. M. Sheldrick, *Acta Cryst. Sect. C*. 2015, **71**, 3-8.
4. D. V. Konarev, A. V. Kuzmin, R. S. Galkin, S. S. Khasanov, R. F. Kurbanov, A. Otsuka, H. Yamochi, H. Kitagawa, R. N. Lyubovskaya, *Z. Anorg. Allg. Chem.* 2019, **645**, 472–483.
5. R. Peverati, D. G. Truhlar, Phys. Chem. Chem. Phys., 2012, 14, 13171-13174
6. R. Peverati, D. G. Truhlar, Phys. Chem. Chem. Phys., 2012, 14, 16187-16191
7. (a) T. Yanai, D. Tew, N. Handy, Chem. Phys. Lett., 2004, 393, 51-57, (b) S. Grimme, S. Ehrlich, L. Goerigk, J. Comp. Chem., 2011, 32, 1456-1465
8. K. A. Peterson, J. Chem. Phys., 2003, 119, 11099
9. N. B. Balabanov, K. A. Peterson, J. Chem. Phys. 123, 064107 (2005)
10. T. H. Dunning Jr., J. Chem. Phys., 1989, 90, 1007
11. E. D. Glendening, A. E. Reed, J. E. Carpenter and F. Weinhold, NBO, Version 3.1
12. M. J. Frisch, G. W. Trucks, H. B. Schlegel, G. E. Scuseria, M. A. Robb, J. R. Cheeseman, G. Scalmani, V. Barone, B. Mennucci, G. A. Petersson, H. Nakatsuji, M. Caricato, X. Li, H. P. Hratchian, A. F. Izmaylov, J. Bloino, G. Zheng, J. L. Sonnenberg, M. Hada, M. Ehara, K. Toyota, R. Fukuda, J. Hasegawa, M. Ishida, T. Nakajima, Y. Honda, O. Kitao, H. Nakai, T. Vreven, J. A. Montgomery Jr., J. E. Peralta, F. Ogliaro, M. Bearpark, J. J. Heyd, E. Brothers, K. N. Kudin, V. N. Staroverov, T. Keith, R. Kobayashi, J. Normand, K. Raghavachari, A. Rendell, J. C. Burant, S. S. Iyengar, J. Tomasi, M. Cossi, N. Rega, J. M. Millam, M. Klene, J. E. Knox, J. B. Cross, V. Bakken, C. Adamo, J. Jaramillo, R. Gomperts, R. E. Stratmann, O. Yazyev, A. J. Austin, R. Cammi, C. Pomelli, J. W. Ochterski, R. L. Martin, K. Morokuma, V. G. Zakrzewski, G. A. Voth, P. Salvador, J. J. Dannenberg, S. Dapprich, A. D. Daniels, O. Farkas, J. B. Foresman, J. V. Ortiz,

J. Cioslowski and D. J. Fox, Gaussian 09, Revision E.01, Gaussian, Inc., Wallingford CT, 2013.